

# A Reliability Model of Wind Farm Considering the Complex Terrain and Cable Failure Based on Clustering Algorithm

Wenxia Liu\*, Qi Chen<sup>†</sup>, Yuying Zhang\*, Guobing Qiu\* and Chenghui Lin\*\*

**Abstract** – A reliability model of wind farm located in mountainous land with complex terrain, which considers the cable and wind turbine (WT) failures, is proposed in this paper. Simple wake effect has been developed to be applied to the wind farm in mountainous land. The component failures in the wind farm like the cable and WT failures which contribute to the wind farm power output (WFPO) and reliability is investigated. Combining the wind speed distribution and the characteristic of wind turbine power output (WTPO), Monte Carlo simulation (MCS) is used to obtain the WFPO. Based on clustering algorithm the multi-state model of a wind farm is proposed. The accuracy of the model is analyzed and then applied to IEEE-RTS 79 for adequacy assessment.

**Keywords:** Cable failure, Clustering algorithm, Complex terrain, Reliability model, Wind farm

## 1. Introduction

Recent public concerns on environmental issues associated with conventional fossil resources has motivated an increased interest in the development and use of alternative sources. Wind energy has been widely recognized as an important alternative with the development in modern WT technology. Many countries, e.g. US, China, Germany and Denmark have integrated large scale wind energy into their power systems with incentive politics promoted which ensure the purchase of the wind energy produced in spite of its uncompetitive prices [1-3].

However the stochastic WFPO, depending on the wind, which is intermittent, has become one major difficulty while planning or operation a power system with increasing wind energy penetration. The impact of wind farms (WFs) on composite power system reliability is a major concern, especially after a series of large scale accidents of wind farms disconnected with the power grid occurred in China since 2011 [4]. The intermittent nature of wind speed, along with the probabilistic behavior of outage of WTs and other components, makes output power of wind farms completely stochastic and different from those of conventional units. Therefore, one of the complexities of integration of wind power in power systems can be seen in the reliability model of wind farms.

Traditionally, the analytic and MCS approaches are always used to model the wind farm [5-11]. Generally a wind farm can be simplified to an equivalent multi-state

unit [7, 10-11], which can be used for reliability evaluation of a power system with wind farms.

Analytic approach is always used when the wind farm is not large. Sayas combines the stochastic characteristics of wind speed with the operational information of the turbines, such as the failure and repair rates, representing the wind farm by a Markov process [5]. Leite utilizes the model for reliability studies, providing an annual estimate of energy production and calculate several performance indexes [6]. Then, based on Markov process Dobakhshari models a wind farm like a multistate conventional unit [7].

Although the model is more credible and reliable, with the wind energy integrated into the power grid in large scale the problem becomes more complex and difficult, especially after incorporating wake effect and other relevant factors in a Markov process.

Roy Billinton proposed MCS to mimic the operation of a wind farm hourly, taking into account the fluctuating characteristics of wind speeds, the random failure of generating units and other recognized factors [8]. Based on the model, assessment of risk-based capacity is carried out for the power system including wind farms [9]. In 2006 Karki and Billinton, etc. presents a simplified multi-state unit model for reliability evaluation of power systems [10]. And the method is further simplified by determining the reasonable multistate representation for a wind farm generation model in reliability evaluation.

Compared with the analytical one, MCS is more applicable to model the wind farm with numerous WTs and always used in an existing composite power grid. Thus, in this paper MCS is selected. The wind farm model is mainly determined by the random nature of the site resource, the characteristic of WTPO, and the unavailability of the WT expressed by the unit forced outage rate (FOR) [8-11]. However, two main aspects should be further investigated:

1. More factors should be taken into account due to the

<sup>†</sup> Corresponding Author: State Key Laboratory of Alternate Electrical Power System with Renewable Energy Sources, School of Electrical and Electronic Engineering, North China Electric Power University, Beijing, China. (qichantd@163.com).

\* State Key Laboratory of Alternate Electrical Power System with Renewable Energy Sources, School of Electrical and Electronic Engineering, North China Electric Power University, Beijing, China.

\*\* Guizhou Electric Power Research Institute, Guiyang, China.

Received: November 18, 2013; Accepted: July 29, 2014

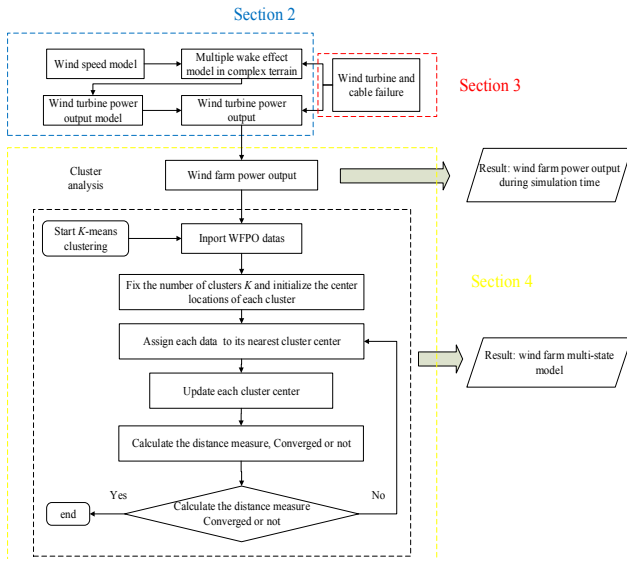


Fig. 1. The overall idea of this paper

differences between wind farms.

2. How to achieve the tradeoff between accuracy and the number of states.

The existing models consider only the wake effect of a wind farm in a flat area. Based on the relatively simple Jensen model, a partial wake effect model in flat terrain between WTs is established [12-14]. When the wind passes over a mountainous land, complex terrain feature will change the wind speed. Wind speed over a mountain is much different from that on a flat area. Therefore wake effect model in flat terrain is not sufficient to accurately evaluate power outputs of WTs at different parts of a wind farm. The terrain influence of a mountainous land on wind speed has not been considered in an adequacy study of a wind farm. Besides, the internal connection line failures in the wind farm have been recognized as a contributing factor to wind power system reliability, after three accidents of a cable breakdown in wind farms and the impact of it on wind farm reliability is investigated. In this paper the number of states and the accuracy of the model is investigated, providing a reference to the tradeoff. The overall idea of the paper is illustrated in Fig. 1.

## 2. Wind Turbine Power Output Considering Multiple Wake Effect in Complex Terrain

### 2.1 Wind speed model

The probability density function (PDF) of wind speed is important in numerous wind energy applications. A large number of studies have been published in scientific literature related to renewable energies that propose the use of a variety of PDFs to describe the wind speed frequency distributions, such as Weibull, Rayleigh,  $r^2$  and so on [15].

Amongst the various distributions, the two parameter Weibull distribution has been the most widely used, accepted and recommended distribution on wind energy [16]. In this paper, two parameter Weibull distribution is used to simulate the wind speed probability distribution, its probability density function (PDF) is given by [17]:

$$f(v) = \left(\frac{k}{c}\right) \left(\frac{v}{c}\right)^{k-1} \exp\left[-\left(\frac{v}{c}\right)^k\right] \quad (1)$$

where  $c$  is the scale factor and  $k$  is the shape factor. Seasonal patterns of wind speed which significantly affect the reliability indexes is taken into account [6]. The values of  $c$  and  $k$  can be estimated using maximum likelihood method based on measured wind speeds [16], [18].

Cumulative distribution function (CDF) of two parameter Weibull distribution is given by:

$$F(v) = 1 - \exp\left[-\left(\frac{v}{c}\right)^k\right] \quad (2)$$

### 2.2 Partial wake effect model in complex terrain

WTs generate electricity by tapping into the energy in the wind. Consequently, the wind leaving the turbine must have a lower energy content than that arriving in front of the turbine [14]. In this paper, a detail wake model, considering partial and multiple wakes inside a wind farm, has been developed.

The Jensen wake model is a single wake model, which demonstrates linear expansion of the wake diameter, ignoring the changes of the wind speed caused by the altitude difference between the WTs. Fig. 2 shows an overview of the wake model.

When completely located in the wake of the upstream WT, the wind speed at location  $x$  is expressed by [14]:

$$\begin{aligned} v(x) &= v_0(1 - d_F) \\ &= v_0[1 - (1 - \sqrt{1 - C_T})\left(\frac{r_0}{r}\right)^2] \end{aligned} \quad (3)$$

where  $v_0$  is the original wind speed,  $d_F$  is the declining coefficient of wind speed in flat terrain,  $C_T$  is the thrust

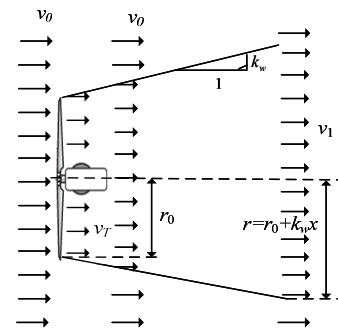


Fig. 2. The Jensen wake model

coefficient,  $r=r_0+k_w x$ ,  $r$  is the wake effect radius,  $k_w$  depends on the terrain and environment,  $k_w=0.04$  for nature wind, otherwise  $k_w=0.08$  [14].

However; the wake effect model in a more general terrain should be proposed for the wind farm located in mountainous land where the difference of altitude between WTs is not negligible. Besides the difference of altitude and the wind direction may probably lead to the downstream WT in partial wake. Combining the basic theories of Jensen model and Lissaman model [19], a partial wake effect model of WTs at the different altitudes in complex terrain is developed in this paper.

In a wind farm configuration, the wind speed at WT  $j$  is affected not only by the upstream WT that is directly in front of it, WT  $i$ , but also by other upstream WTs [14]. At first, only the effect on WT  $j$  caused by WT  $i$  is studied in this section. In a wind farm, the relative position of WT  $i$  and WT  $j$  is assumed to be shown in Fig. 3. In the figure,  $h_i$  and  $h_j$  are the rotor altitudes of WT  $i$  and WT  $j$ ,  $r_i$  and  $r_j$  are the rotor radii of WT  $i$  and WT  $j$  and  $x_{ij}$  is the distance between WT  $i$  and WT  $j$ . Then the wind speed of WT  $j$  affected by WT  $i$  can be calculated using the following expression:

$$v_{j(i)} = v_i [1 - (1 - \sqrt{1 - C_T}) \cdot (\frac{h_i}{h_j})^{2\alpha} \cdot (\frac{r_j}{r_i(x_{ij})})^2 \cdot (\frac{A_{shad,ij}}{A_{rotor}})] (\frac{h_j}{h_i})^\alpha \quad (4)$$

where  $v_i$  and  $v_{j(i)}$  are the wind speeds at WT  $i$  and WT  $j$ ;  $\alpha$  is the coefficient of wind speed variation with the altitude, which is generally 1/7.  $r_i(x_{ij})$  is the wake effect radius at WT  $j$  caused by WT  $i$ ;  $r_i(x_{ij})=r_i+k_w x_{ij}$ ;  $A_{rotor}$  is the area covered by the rotor of downstream WT  $i$ ,  $A_{rotor}=\pi r_j^2$ ;  $A_{shad,ij}$  is the area projected by downstream WT  $j$  in the wake region of upstream WT  $i$ , which can be calculated through the following expression:

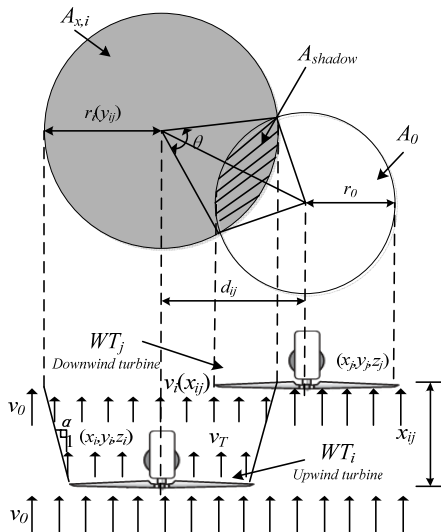


Fig. 3. Partial block wake effect model

$$A_{shad,ij} = r_i^2(x_{ij}) \cos^{-1} \left( \frac{r_i^2(x_{ij}) + d_{ij}^2 + \Delta h^2 - r_j^2}{2r_i(x_{ij}) \cdot \sqrt{\Delta h^2 + d_{ij}^2}} \right) + r_j^2 \cos^{-1} \left( \frac{r_j^2 + d_{ij}^2 + \Delta h^2 - r_i^2(x_{ij})}{2r_j \cdot \sqrt{\Delta h^2 + d_{ij}^2}} \right) - r_i(x_{ij}) \cdot \sqrt{\Delta h^2 + d_{ij}^2} \cdot \sin[\cos^{-1} \left( \frac{r_i^2(x_{ij}) + d_{ij}^2 + \Delta h^2 - r_j^2}{2r_i(x_{ij}) \cdot \sqrt{\Delta h^2 + d_{ij}^2}} \right)] \quad (5)$$

where  $\Delta h=|h_j-h_i|$ ;  $d_{ij}$  is the horizontal spacing between WT  $i$  and WT  $j$ . When  $\Delta h=|h_i-h_j|=0$  and  $A_{shad,ij}=A_{rotor}$ , it turns to be the complete wake effect model in flat terrain expressed by Eq. (3).

### 2.3 Multiple wake effect model in complex terrain

It is quite possible that one WT is affected by a multiple wake effect in a wind farm containing a large number of WTs. Therefore the multiple wake effect model in complex terrain should be taken into account. This model assumes that the kinetic energy deficit of interacting wakes is equal to the sum of the energy deficits of the individual wakes [20]. Thus, the velocity at the intersection of several wakes can be calculated using the following expression:

$$1 - \frac{v_{eq,j}}{v_{j0}} = \sqrt{\sum_{i=1}^N (1 - \frac{v_{j(i)}}{v_{j0}})^2} \quad (6)$$

where  $v_{j0}$  is the wind speed at WT  $j$  without any wake effect;  $N$  is the total number of upwind influencing turbines;  $v_{eq,j}$  is the wind speed at WT  $j$  such that all the wakes are taken into account;  $v_j$  is the wind speed at WT  $j$  affected by the individual WT  $i$ .

### 2.4 Wind turbine power output model

The WTPO is a function of the wind speed. The randomness of wind speed determines the WTPO. The relationship between the WTPO and the wind speed is non-linear due to the combined effects of aero-turbine and generator characteristics [21]. However, the assumption of the linear characteristic of the WTPO with the wind speed simplifies the calculations without roughly errors. Ignoring the differences between WT types, the commonly used linear relationship between the WTPO and the wind speed can be calculated using the following expression [22]:

$$P_w = \begin{cases} 0, & v > v_{co} \text{ or } v < v_{ci} \\ k_1 v + k_2, & v_{ci} \leq v \leq v_r \\ P_r, & v_r \leq v \leq v_{co} \end{cases} \quad (7)$$

where  $P_r$ ,  $v_{ci}$ ,  $v_r$  and  $v_{co}$  are the rated power output, the cut-in wind speed, the rated wind speed, and the cut-out wind speed of the WT, respectively;  $k_1 = P_r / (v_r - v_{ci})$ ;  $k_2 = -k_1 v_{ci}$ .

### 3. Wind Farm Reliability Model

#### 3.1 Wind farm element reliability model: Connection lines and wind turbines

Generally, four main parts: WTs, package transformers, collection lines, substations constitute the wind farm. In present techniques, the impact of connection line reliability to wind farms has not been considered in wind farms reliability modeling. The lines, which are long with high failure rates and are used for collecting and delivering energy, have a great impact on the wind farm. A series of large scale accidents of wind farms disconnected with the power grid occurred in China since 2011 just due to the breakdown of cable [4].

#### 3.2 The reliability model of the connection line

The model of cable is investigated in this section as an example, but the model is also applicable to common connection lines like overhead line. Electric power network topology in the wind farm comprises 3 general forms: chain, ring and star [23]. Two-state model is applied to each cable, representing the operation (up) and outage (down) state. The Markov chain of cable is illustrated in Fig. 4, where  $\lambda_{cable}$ ,  $\mu_{cable}$  are failure rate and repair rate.

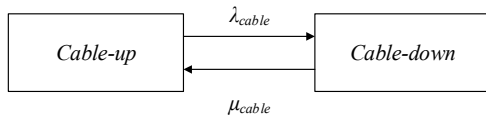


Fig. 4. Markov chain model of the cable

The probability calculated from the Markov chain above is as follows:

$$P_{cable-up}(t) = \frac{\mu_{cable}}{\lambda_{cable} + \mu_{cable}} + \frac{\lambda_{cable}}{\lambda_{cable} + \mu_{cable}} e^{-(\lambda_{cable} + \mu_{cable})t} \quad (8)$$

$$P_{cable-down}(t) = \frac{\lambda_{cable}}{\lambda_{cable} + \mu_{cable}} - \frac{\lambda_{cable}}{\lambda_{cable} + \mu_{cable}} e^{-(\lambda_{cable} + \mu_{cable})t} \quad (9)$$

Only long-term state probabilities are of interest, the normal and failure state probabilities of each component are expressed as follows:

$$P_{cable-up}(\infty) = \frac{\mu_{cable}}{\lambda_{cable} + \mu_{cable}} \quad (10)$$

$$P_{cable-down}(\infty) = \frac{\lambda_{cable}}{\lambda_{cable} + \mu_{cable}} \quad (11)$$

#### 3.3 The Reliability of the Wind Turbine

Operation of the WT is affected by the connecting cable. Some outage of the WTs is due to the cable failure and the equivalent outage of WTs increase. The model of the WTs is illustrated below.

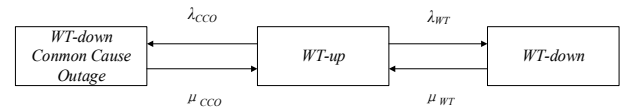


Fig. 5. Markov chain model of the WT

The common cause outage indicates the WT outage due to the cable failures. The WT outage caused by the failure itself is alone to be separated from the common cause outage. The probability of WT being available  $P'_{WT_i}$  can be calculated below:

$$P'_{WT_i} = P_{WT_i} \times (1 - \sum_{f \in Fi} P_{cable-down,f}) \quad (12)$$

Where  $P'_{WT_i}$  is the equivalent availability of the  $i$ th WT considering the common cause outage,  $P_{WT_i}$  is the availability of the  $i$ th WT,  $Fi$  is a failure set which makes the  $i$ th WT unavailable due to the common cause of cable,  $f$  represents a failure that belongs to  $Fi$ .

Fig. 6 below shows 10 WTs connected to the bus in chain form.

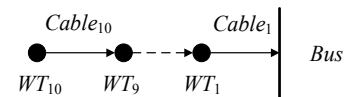


Fig. 6. Chain form of the WTs

The equivalent availability of each turbine is demonstrated below in Fig. 7.

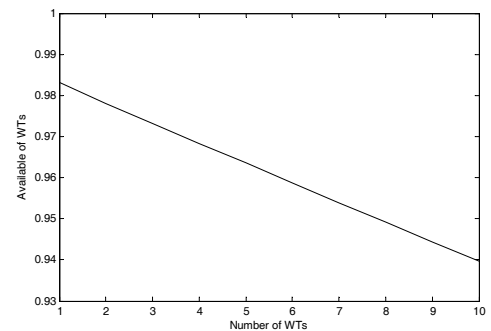


Fig. 7. Equivalent availability of the WTs

As it is seen in the figure above, the equivalent availability decreases with the number of cables used to connect into the grid increases.

#### 4. Wind Farm Multi-State Probabilistic Model Based On K-Means Clustering

##### 4.1 Wind farm power output

The MCS is proposed to mimic the WFPO. The step of the calculation is as follows:

- 1) Input the location coordinates of each WT.
- 2) Generate the wind speed and wind direction.
- 3) Obtain the state of WTs and cables according to MCS.
- 4) Calculate the equivalent wind speed at each location of WT, especially the WT in the state of outage does not impact the WTs downstream.
- 5) Calculate all the WTPO according to the equivalent wind speed.
- 6) Calculate the WFPO.
- 7) Determine whether it is the end of the simulation time. If it is, end the simulation and generate the output. If not, return to step 2).

##### 4.2 Multi-State probabilistic model based on clustering

In order to apply time series WFPO simulated hourly to power system reliability evaluation, the multi-state probabilistic model is obtained through clustering the WFPO data.

Clustering is a process of partitioning or grouping a set of data objects into a number of clusters such that similar patterns are assigned to one cluster [24]. *K*-means clustering is one of the simplest unsupervised learning algorithms that solve the well-known clustering problem. In this paper, *K*-means clustering will be used to partition a time series of WFPO into *K* different clusters and the wind farm will be equivalent to a *K*-state conventional unit.

The *K*-means clustering attempts to find the cluster centers ( $\mathbf{c}_1, \mathbf{c}_2, \dots, \mathbf{c}_K$ ) such that the sum of the squared distances (called Distortion) of each data point ( $\mathbf{x}_i$ ) to its nearest cluster center ( $\mathbf{c}_k$ ) is minimized, as shown by following expression:

$$\text{Distortion, } Dis = \sum_{i=1}^n [\min_{k=1,2,\dots,K} d(\mathbf{x}_i, \mathbf{c}_k)]^2 \quad (13)$$

where  $d(\mathbf{x}_i, \mathbf{c}_k)$  is the Minkowski distance function and its expression is given by:

$$d(\mathbf{x}_i, \mathbf{c}_k) = \|\mathbf{x}_i - \mathbf{c}_k\|_p = \left( \sum_{j=1}^m (x_{ij} - c_{kj})^p \right)^{1/p} \quad (14)$$

where  $p$  is a positive integer;  $m$  is the dimension of vector  $\mathbf{c}_k$ .

Typically  $d(\mathbf{x}_i, \mathbf{c}_k)$  is chosen as the Euclidean distance, which is a special case ( $p=2$ ) of the Minkowski distance.

The *K*-means clustering includes the following steps [24]:

- 1) Fix the number of clusters *K* and initialize the center locations of each cluster, ( $\mathbf{c}_1^{(0)}, \mathbf{c}_2^{(0)}, \dots, \mathbf{c}_K^{(0)}$ ). Each cluster center is a *m*-dimensional vector i.e.,  $\mathbf{c}_i^{(0)} = \{c_{i1}^{(0)}, c_{i2}^{(0)}, \dots, c_{im}^{(0)}\}$ .
- 2) Start the iterative procedure. Set the iteration count  $t=1$ .
- 3) Calculate the distance measure,  $d_{ki}^{(t-1)}$ , between *k*th cluster center and *i*th data set (data point in *m*-space). The distance measure used is Euclidean distance as given by Eq. (15).

$$d_{ki}^{(t-1)} = \|\mathbf{x}_i - \mathbf{c}_k^{(t-1)}\|_2 = \left( \sum_{j=1}^m (x_{ij} - c_{kj}^{(t-1)})^2 \right)^{1/2} \quad (15)$$

- 4) Assign each data object  $\mathbf{x}_i$  to its nearest cluster center  $\mathbf{c}_k$ .
- 5) Update each cluster center  $\mathbf{c}_k^{(t)}$  as the mean of all  $\mathbf{x}_i$  that have been assigned as closest to it as given by Eq. (16).

$$\mathbf{c}_k^{(t)} = \sum_{\mathbf{x}_i \in k} \mathbf{x}_i / n_k \quad (16)$$

where  $n_k$  is the number of data items belonging to *k*th cluster.

- 6) Calculate the Distortion *Dis* as given by Eq. (13). This function depicts the sum of all intra cluster distances, which is lower the better.
- 7) If the value of *Dis* has converged, return the final cluster centers ( $\mathbf{c}_1^{(t)}, \mathbf{c}_2^{(t)}, \dots, \mathbf{c}_K^{(t)}$ ). Else set  $t=t+1$  and go to (3).

## 5. Example Analysis

### 5.1 Relevant data of wind farm

In this paper, a wind farm containing 2MW WTs with a total of 160MW installed (the main technical parameters of the WT are given in Table 1 [25].) is selected as an example to do the relevant research and its specific layout is shown in Fig. 8. The topography of the wind farm is complex and the rotor altitude of each WT varies. The wind speed and wind direction of the wind farm are measured by the anemometer tower, which is at the altitude of 70 m. Besides, the data next to the WT in Fig. 8 is the rotor altitude of the WT.

Due to the randomness of wind direction, wind rose is used to describe the wind direction. And the wind rose of the selected wind farm is shown in Fig. 9. In this paper,

**Table 1.** The main technical parameters of asynchronous wind turbine

$r_0$	$v_{ci}$	$v_r$	$v_{co}$	$P_r$	$h$
45m	3m/s	12m/s	25m/s	2MW	60m

two-parameter Weibull distribution is used to simulate the wind speed. Thus, assuming the values of  $c$  and  $k$  change monthly, the values of  $c$  and  $k$  from Capo Vado wind farm in [26] are used for further analysis in this paper and the values of  $c$  and  $k$  are presented in Table 2.

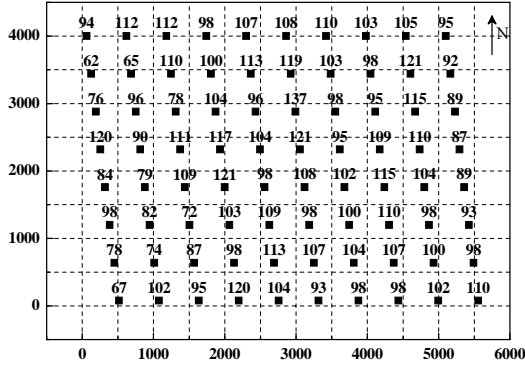


Fig. 8. The layout of wind turbines in wind farm

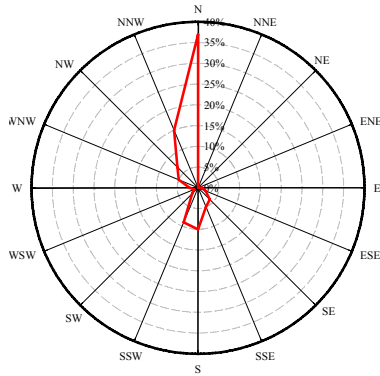


Fig. 9. Wind rose of the wind farm

Table 2. Monthly Weibull parameters for Capo Vado site

Month	$c(m/s)$	$k$	Month	$c(m/s)$	$k$
JAN	7.5	1.36	JUL	5.13	1.86
FEB	7.15	1.63	AUG	4.97	1.83
MAR	7.05	1.46	SEP	5.61	1.54
APR	6.21	1.3	OCT	6.51	1.48
MAY	5.42	2.03	NOV	7.04	1.44
JUN	5.53	1.89	DEC	8.62	1.39

Table 3. Multistate wind farm power output probability distribution models

6-state		7-state		8-state		9-state		10-state	
$P_{out}/p.u.$	Prob.	$P_{out}/p.u.$	Prob.	$P_{out}/p.u.$	Prob.	$P_{out}/p.u.$	Prob.	$P_{out}/p.u.$	Prob.
0.0132	0.5825	0.0077	0.5128	0.0074	0.5093	0.0049	0.4654	0.0041	0.4485
0.1192	0.1922	0.0752	0.1715	0.0730	0.1689	0.0526	0.1534	0.0463	0.1492
0.2672	0.0913	0.1632	0.1116	0.1568	0.1103	0.1104	0.1011	0.0986	0.1038
0.4498	0.0531	0.2903	0.0751	0.2704	0.0692	0.1788	0.0778	0.1659	0.0872
0.6533	0.0363	0.4616	0.0497	0.4026	0.0428	0.2823	0.0645	0.2628	0.0604
0.9134	0.0446	0.6590	0.0350	0.5507	0.0350	0.4153	0.0416	0.3663	0.0367
—	—	0.9143	0.0442	0.7203	0.0242	0.5636	0.0341	0.4826	0.0324
—	—	—	—	0.9251	0.0403	0.7338	0.0229	0.6169	0.0267
—	—	—	—	—	—	0.9280	0.0391	0.7762	0.0193
—	—	—	—	—	—	—	—	0.9360	0.0357

## 5.2 Modeling of wind farm power output probability distribution

Using a 50-year time series of wind speed and wind direction simulated hourly, a time series of power output of the wind farm (seen in Fig. 8) is calculated with a multiple wake effect model in complex terrain taken into consideration. With  $K$ -means clustering used to divide the time series of power output of the wind farm into  $K$  ( $K=6,7,8,9,10$ ) different clusters, multistate WFPO probability distribution models is shown in Table 3.

Table 3 shows that the wind farm mentioned in Section 5.1 is equivalent to a (6~10)-state conventional unit. And the maximum of WFPO increases with the increase of the state number; however, its corresponding probability decreases.

In order to study the accuracies of using (6~10)-state WFPO probability distribution models to simulate the WFPO, the error curves of comparing the simulated power output with the actual power output of the wind farm are plotted in Fig. 10.

From Fig. 10, it can be noted that the errors between the simulated power output and the actual power output of the wind farm are volatile, but the overall errors are all less than 1% when the simulation times is about 50% of the total simulation times (438,000 times, 50 years, simulating hourly). Compared with the mean and standard deviation of the time series of the actual WFPO calculated in Fig. 10 when the simulation times is 438,000, the errors of the means and standard deviations of the simulated time series

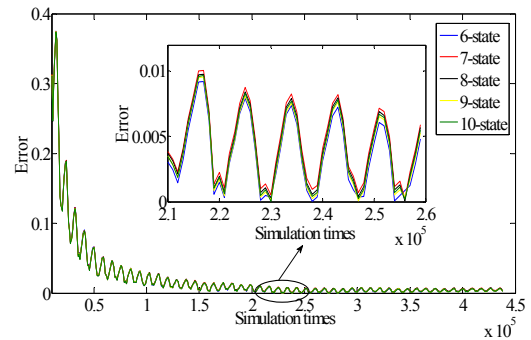
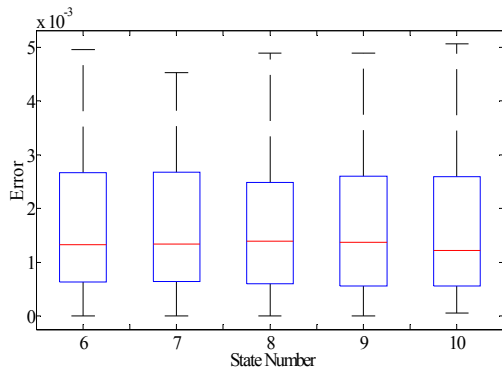


Fig. 10. Error curves of multistate wind farm power output probability distribution models

**Table 4.** Errors of the mean and standard deviation of every multistate model

State Number	Mean (%)	Standard deviation (%)
6	0.2867	0.7558
7	0.3488	0.4464
8	0.3088	0.2904
9	0.2702	0.2282
10	0.2737	0.1084

**Fig. 11.** Boxplot of every multistate model

of the WFPO are shown in Table 4.

Combining with Fig. 10 (when the simulation times is 438,000, the errors of (6~10)-state models:  $7 > 8 > 6 > 10 > 9$ ) and Table 4, the means reflect the accuracy rate of the multistate models and the standard deviations are related to the volatility of the multistate models to simulate WFPO. Because of the probability in the process of simulation, the accuracy rates of the multistate models do not increase with the state number, but do the volatility of the multistate models.

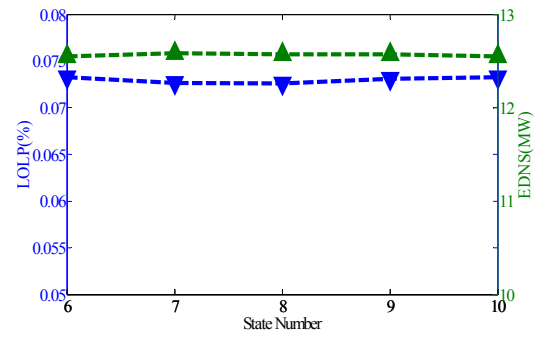
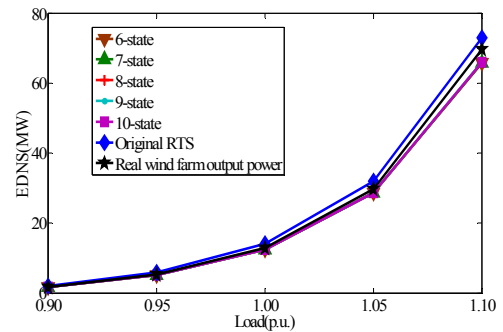
Due to the uncertainties of the simulation accuracies of the (6~10)-state models, boxplot is used to describe the volatility of the error of every multistate model in simulating WFPO (seen in Fig. 11). The boxplot is obtained through using every multistate model to simulate WFPO for 100 simulations (the time of every simulation is 50 years).

As it can be seen from Fig. 11, the average error of every multistate model in simulating WFPO varies from 0.1% to 0.2% and the maximum error is not more than 0.5%. Therefore, every multistate model can ensure its reliability and accuracy when simulating WFPO. In other words, the multistate models can effectively simulate WFPO.

### 5.3 Wind farm adequacy assessment

In this paper, the IEEE-RTS 79 [27] Test System with the wind farm (in Section 5.1) integrated into the 16th node is applied to carry out the adequacy assessment. And the multistate models (seen in Table 3) are used to simulate the WFPO to investigate the impact of multistate models on the IEEE-BTS 79 generating system adequacy. The reliability indexes LOLP (Lost of Load Probability) and EDNS (Expected Demand Not Supplied) are calculated for the corresponding analysis.

Fig. 12 shows the results of LOLP and EDNS calculated

**Fig. 12.** LOLP and EDNS of every multistate model**Fig. 13.** Curves of EDNS with the various annual peak loads

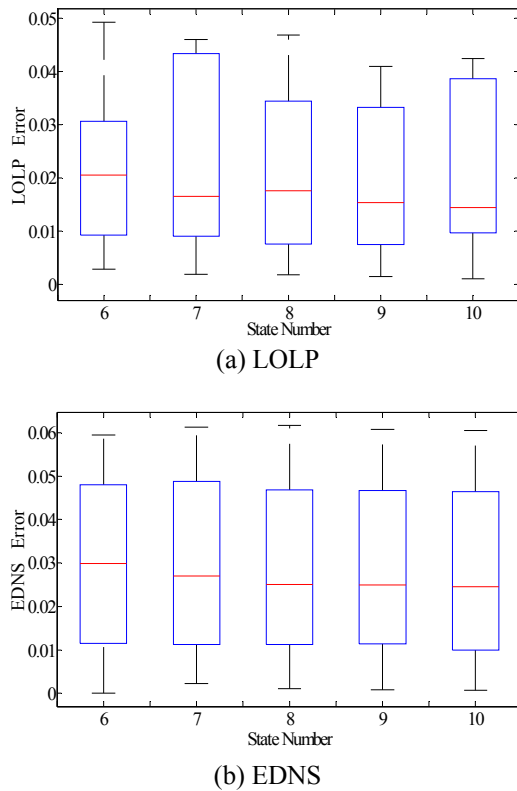
using (6~10)-state models to simulate WFPO. In Fig. 12, the LOLP and EDNS both fluctuate slightly with the state number, basically in accord with the reliability impact of the actual WFPO on the original test system.

Fig. 13 shows the values of EDNS change with the various annual peak loads ranging from 0.9p.u. to 1.1p.u. (the peak load of the test system is 2850 MW) with (6~10)-state models integrated into the test system. It can be seen from Fig. 13 that the values of EDNS are relatively close, using a model with six or more states to represent the wind farm. The differences between the EDNS using the actual WFPO and the EDNSs using (6~10)-state models to represent the wind farm are relatively small but increase with the various annual peak loads ranging from 0.9p.u. to 1.1p.u..

From above analysis, the multistate models can be used to represent wind farm in reliability evaluation of a power system with wind farms.

In order to analyze the accuracies of using multistate models to represent wind farm in reliability evaluation of a power system with wind farms, the boxplots of LOLP error and EDNS error are obtained through 50 simulations (the time of every simulation is 50 years) (seen in Fig. 14). The errors of LOLP or EDNS are calculated between the one calculated using the actual WFPO and the ones calculated using (6~10)-state models to represent the wind farm in the reliability evaluation of a power system with wind farms.

Fig. 14 shows that the average error of LOLP is volatile (varies between 1% and 2%) and the maximum error is not more than 5%; the average error of EDNS decreases with the increasing state number (varies between 2% and 3%) and the maximum error is not more than 7%. Therefore, the



**Fig. 14.** Boxplots of LOLP error and EDNS error

multistate models can effectively represent wind farm in reliability evaluation of a power system with wind farms and ensure the accuracy.

## 6. Conclusion

This paper has introduced a modeling approach for WFPO probability distribution based on clustering algorithm. Firstly, combining the basic theories of Jensen model and Lissaman model, a partial wake effect model of WTs at the different altitudes in complex terrain is established. A wind farm reliability model, especially considering the outage of wind farm internal connection lines is set up in this paper. Finally, after an introduction of  $K$ -means clustering in detail, a wind farm can be equivalent to a multi-state conventional unit with  $K$ -means clustering as a method.

Taking an installed capacity of 160 MW wind farm as an example, it turns out that the multistate models can effectively simulate the WFPO. The studies on the IEEE-RTS 79 Test System, with reliability indexes LOLP and EDNS calculated, indicate that the multistate models can also effectively represent wind farm in reliability evaluation of a power system with wind farms and ensure the accuracy.

## Acknowledgements

This work was supported by a grant from the National

High Technology Research and Development Program of China (863 Program) (No.2013BAA02B00).

## References

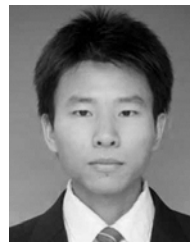
- [1] Keyhani, et al. "An assessment of wind energy potential as a power generation source in the capital of Iran, Tehran," *Energy*, vol. 35, no. 1, pp. 188-201, 2010.
- [2] J. Xu, D. He and X. Zhao, "Status and prospects of Chinese wind energy," *Energy*, vol. 35, no. 11, pp. 4439-4444, 2010.
- [3] K. Sperling, F. Hvellund and BV. Mathiesen, "Evaluation of wind power planning in Denmark-towards an integrated perspective," *Energy*, vol. 35, no. 12, pp. 5443-5454, 2010.
- [4] L. Zhang and W. Qiu, "Consideration of Large-scale Wind Farm Disconnection from Grid," *Electric Power Construction*, vol. 33, no. 3, pp. 11-14, 2012.
- [5] F. Castro Sayas and R. N. Allan, "Generation availability assessment of wind farms," *Generation, Transmission and Distribution, IEE Proceedings*, Vol. 143. No. 5. IET, 1996.
- [6] A.S. Dobakhshari and M. Fotuhi-Firuzabad, "A reliability model of large wind farms for power system adequacy studies," *Energy Conversion, IEEE Transactions on*, vol. 24, no. 3, pp. 792-801, 2009.
- [7] P. Leite, Andréa, C. L. Borges, and D. M. Falcao, "Probabilistic wind farms generation model for reliability studies applied to Brazilian sites," *IEEE Trans. Power Systems*, vol. 21, no. 4, pp. 1493-1501, 2006.
- [8] R. Billinton, H. Chen and R. Ghajar, "A sequential simulation technique for adequacy evaluation of generating systems including wind energy," *Energy Conversion, IEEE Transactions on*, vol. 11, no. 4, pp. 728-734, 1996.
- [9] R. Billinton and H. Chen, "Assessment of risk-based capacity benefit factors associated with wind energy conversion systems," *Power Systems, IEEE Transactions on*, vol. 13, no. 3, pp. 1191-1196, 1998.
- [10] R. Karki, P. Hu and R. Billinton, "A simplified wind power generation model for reliability evaluation," *Energy conversion, IEEE Transactions on*, vol. 21, no. 2, pp. 533-540, 2006.
- [11] R. Billinton and Y. Gao, "Multistate wind energy conversion system models for adequacy assessment of generating systems incorporating wind energy," *Energy Conversion, IEEE Transactions on*, vol. 23, no. 1, pp. 163-170, 2008.
- [12] H. WANG and X. BAI, "Assessment on generation adequacy and capacity credit for large-scale wind farm," *Power System Technology*, vol. 6, pp. 036, 2012.
- [13] N. O. Jensen, *A note on wind generator interaction*, 1983.
- [14] F. González-Longatt, P. Wall and V. Terzija, "Wake effect in wind farm performance: Steady-state and dynamic behavior," *Renewable Energy*, vol. 39, no. 1,

pp. 329-338, 2012.

- [15] J.A. Carta, P. Ramírez and S. Velázquez, "A review of wind speed probability distributions used in wind energy analysis: Case studies in the Canary Islands," *Renewable and Sustainable Energy Reviews*, vol. 13, no. 5, pp. 933-955, 2009.
- [16] S. A. Akdağ and A. Dinler, "A new method to estimate Weibull parameters for wind energy applications," *Energy conversion and management*, vol. 50, no. 7, pp. 1761-1766, 2009.
- [17] Hetzer, John, D. C. Yu, and K. Bhattarai, "An economic dispatch model incorporating wind power," *Energy Conversion, IEEE Transactions on*, vol. 23, no. 2, pp. 603-611, 2008.
- [18] G. Justus, et al, "Methods for estimating wind speed frequency distributions," *Journal of applied meteorology*, vol. 17, no. 3, pp. 350-353, 1978.
- [19] R. ZHENG, et al, "Modeling of Large-Scale Wind Farms in the Probabilistic Power Flow Analysis Considering Wake Effects [J]," *Journal of Xi'an Jiaotong University*, vol. 12, pp. 019, 2008.
- [20] P. G. de and Mikel et al, "Power generation efficiency analysis of offshore wind farms connected to a SLPC (single large power converter) operated with variable frequencies considering wake effects," *Energy*, vol. 37, no. 1, pp. 455-468, 2012.
- [21] J. Wen, Y. Zheng and F. Donghan, "A review on reliability assessment for wind power," *Renewable and Sustainable Energy Reviews*, vol. 13, no. 9, pp. 2485-2494, 2009.
- [22] L. W. Wu, J. H. Zhang and R.X Liu, "A wind farm reliability model considering wind turbine faults and its application," *Automation of Electric Power Systems*, vol. 16, no. 36, pp. 31-35, 2012.
- [23] J. Jin, Q. Ai, L. Xi, etc. al, "Internal electrical wiring system of off-shore wind farms," *East China Electric Power*, vol. 35, no. 10, pp. 20-23, 2007.
- [24] S. Kalyani and K. S. Swarup, "Particle swarm optimization based K-means clustering approach for security assessment in power systems," *Expert Systems with Applications*, vol. 38, no. 9, pp. 10839-10846, 2011.
- [25] Z. Bie, et al, "Studies on models and algorithms of the power system probabilistic production simulation integrated with wind farm," *Power & Energy Society General Meeting, 2009. PES'09. IEEE* (pp.1-7). IEEE.
- [26] Ouammi, et al, "Monthly and seasonal assessment of wind energy characteristics at four monitored locations in Liguria region (Italy)," *Renewable and Sustainable Energy Reviews*, vol. 14, no. 7, pp. 1959-1968, 2010.
- [27] P. M. Subcommittee, "IEEE reliability test system," *Power Apparatus and Systems, IEEE Transactions on*, vol. 6, pp. 2047-2054, 1979.



**Wenxia Liu** She received B.S. degree in Radio technology from Nanjing University of Science and Technology in 1990, and obtained M.S. degree and PhD degree in Electric power system and its automation from Northeast of China Electric Power University and North China Electric Power University in 1995 and 2009 respectively. She is currently associate professor in the school of Electrical and Electronic Engineering, North China Electric Power University, Beijing, China. Her research interests are risk assessment in power system, power system dispatch and management automation



**Qi Chen** He received B.S. degree in electrical engineering from North China Electric Power University in 2013. He is currently a M.S. degree candidate in school of electrical engineering in North China Electric Power University. His major interest lies in the reliability evaluation in power system.



**Yuying Zhang** She received the B.S. degree in electrical engineering from the Southwest Jiaotong University, Chengdu, China, in 2012 and currently working towards the M.S. degree in electrical engineering at North China Electric Power University. Her research interests include active distribution system planning, investment evaluation of smart grid, and reliability theories.



**Guobing Qiu** He received B.S. degree and M.S. degree in electrical engineering from North China Electric Power University in 2011 and 2014. He is currently working in Jinhua electric power corporation. His major interest lies in the reliability modeling in power system.



**Chenghui Lin** He was born in 1983. He received his M.S. degree in Sichuan University. He is working in Guizhou Electric Power Research Institute. His major interest lies in the electric power system and its automation.